6.2

THE LAGRANGE TORNADO DURING VORTEX2. PART I: PHOTOGRAMMETRY ANALYSIS OF THE TORNADO COMBINED WITH SINGLE-DOPPLER RADAR DATA

Roger M. Wakimoto*, Nolan T. Atkins#, and Joshua Wurman+

*National Center for Atmospheric Research
Boulder, CO 80305

#Lyndon State College
Lyndonville, VT 05851

+Center for Severe Weather Research
Boulder, CO 80305

1. INTRODUCTION

A major milestone was reached in the operational detection of severe weather when the hook echo was first observed by radar and shown to be associated with tornadogenesis (Stout and Huff 1953, Forbes 1981). Subsequent studies examining radial velocities based on Doppler radars measurements were able to resolve the mesocyclone and the tornadic-vortex signature (TVS) which are associated with the parent circulation of tornadoes and the tornado, respectively (e.g., Brown et al. 1978). More recently, successful intercepts of supercell storms with mobile Doppler radars have provided unprecedented, close-up views of the structure of the hook echo and the intense circulation within and surrounding the tornado (e.g., Bluestein et al. 1993, 1997, 2004, 2007a&b; Wurman and Gill 2000; Alexander and Wurman 2005; Wurman et al. 2007a&b). One of the characteristics features within the hook echo is the weak-echo hole (WEH), first documented by Fujita (1981). The WEH appears inside the tornado core and is surrounded by a high-reflectivity tube that is wider that the tornado (e.g., Fujita 1981, Wurman et al. 1996, Wakimoto et al. 1996, Wurman and Gill 2000, Bluestein et al. 2004, 2007b) and is likely caused by the centrifuging of hydrometeors and debris (Dowell et al. 2005).

While these past studies have collected a plethora of data on the echo structure and velocity fields in tornadoes, careful analysis of pictures taken at the same time have been relatively rare (Bluestein et al. 1993, 1997, 2004, 2007a&b; Wakimoto et al. 2003). Photogrammetric analysis is important since it provides quantitative information about the tornado (e.g., condensation funnel width) that cannot be accurately determined using a Doppler radar. In addition, few studies have attempted to merge Doppler radar data with tornado photographs. Wakimoto et al. (2003), Dowell et al. (2005), and Rasmussen and Straka (2007) superimposed interpolated radar reflectivity and Doppler velocity data onto a picture of the tornado but only for a single time. Wakimoto and Martner (1992) provided a photogrammetric and Doppler radar analysis of the entire life cycle of a Colorado tornado, however, it was associated with a non-supercell storm (i.e., the storm was not associated with a mesocyclone).

This paper presents an analysis of a tornado that developed near LaGrange, Wyoming on 5 June 2009 during the Verification on the Origins of Rotation in Tornadoes Experiment II (VORTEX2). VORTEX2 was a large multiagency field project operated 10 May - 13 June 2009 focused on collecting high resolution data on tornadoes and tornadic storms (Bluestein et al. 2009). The experiment was unique in that the fleet of instrumentation was mobile during the entire field phase. Facilities included 10 mobile radars, mobile mesonet instrumented vehicles, weather balloon launching vans, photography teams, and other instruments. A number of vehicles traveled over 16,000 km across the southern and central plains while intercepting a number of supercell storms. The primary data set used in this study was collected by the Doppler on Wheels (DOWs).

The LaGrange tornado was scanned by several radars while the evolution of the condensation funnel was captured by a series of photographs. In this paper, single-Doppler radar data are combined with these photographs in an attempt to relate the hook echo, WEH, and rotational couplet to the visual characteristics of the tornado.

2. DATA COLLECTION AND THE HOOK ECHO

Figure 1 shows the initial deployment of DOW6 and DOW7 along a north-south oriented highway in Wyoming in order to collect dual-Doppler data. The radars were separated by ~15 km. Still photographs were taken at the same location as the radars as schematically illustrated in the figure. The hook echo at 4 times based on low-level scans by the DOWs is plotted on the figure. A more complete presentation of the evolution of the hook echo from 2156:08 – 2216:07 is shown in Fig. 2. A WEH is apparent in most of the low-level scans. The center of the rotational couplet that is evident in Fig. 2 was plotted on Fig. 1 and reveals the non-linear path that the circulation followed until it dissipated soon after crossing Highway 85. The motion of the couplet was ~280° at speeds that ranged between 9.1 - 9.6 m s^{-1}. Accordingly, the azimuths labeled on photos A, B, and C in Fig. 1 reveal that the tornado was heading toward DOW7.

The surrounding terrain was hilly and relatively barren. As a result, the tornado did not cause significant damage which was confirmed based on a post-storm survey. A ground survey on 6 June followed by an aerial survey on 8 June, however, revealed a few downed trees, broken branches, and snapped telephone poles as shown in Fig. 1. The documented damage and radial velocities recorded by the DOWs resulted in EF2 rating for this tornado by the National Weather Service. The

* *Corresponding author address: Roger M. Wakimoto, National Center for Atmospheric Research, P.O. Box 3000, Boulder, CO 80307; e-mail: wakimoto@ucar.edu*

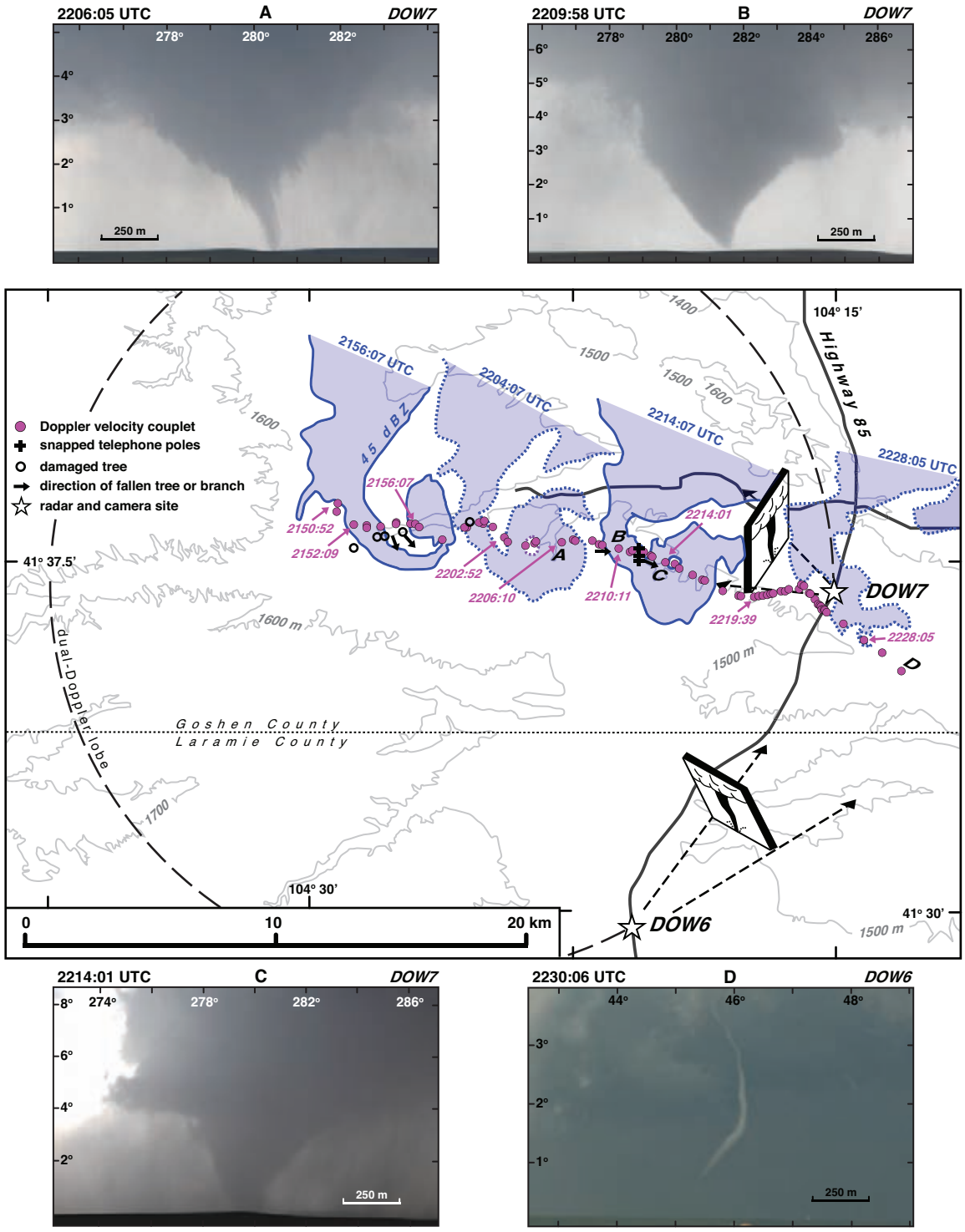

Fig. 1. Hook echo (1° elevation angle) associated with the La Grange supercell storm at 2156:07, 2204:07, 2214:07, and 2228:05 UTC recorded from the Doppler on Wheels (DOWs). Magenta dots represent the location of the tornadic rotational couplet based on low-level scans. Camera sites were collocated with the radars as schematically shown in the figure. Damage to telephone poles and trees are plotted (explanation of the symbols are shown in the legend). Photographs of the tornado at 4 locations along the track are shown (letter identifiers are plotted along the track). Photos A, B, and C were taken from the DOW6 location while D was taken from the DOW7 site. Photos were photogrammetrically enlarged or reduced so that the relative dimensions of the tornado can be estimated. The locations of DOW6 and DOW7 are shown by the stars. The primary dual-Doppler lobe is plotted.

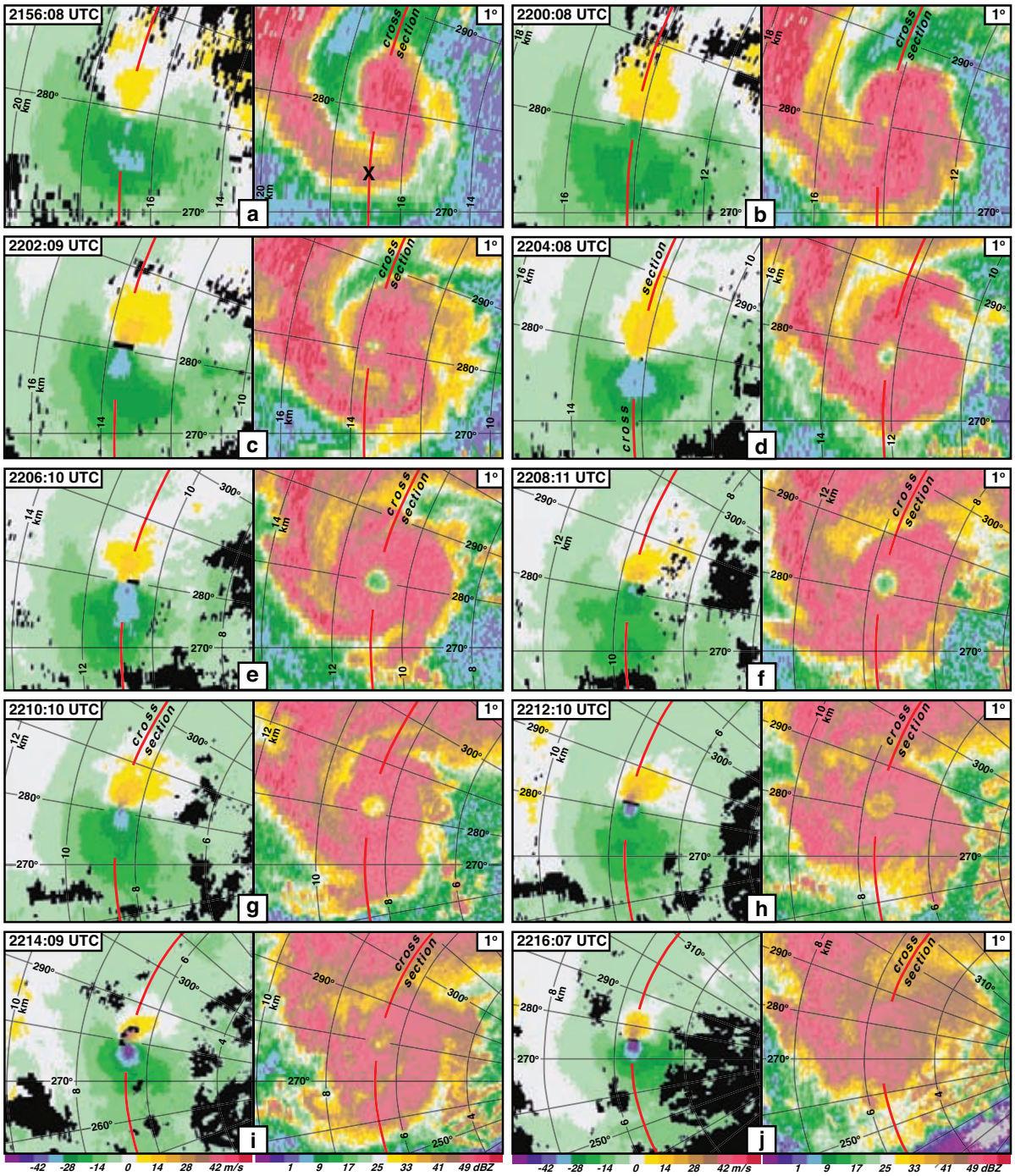

Fig. 2. A series of radar reflectivity and single-Doppler velocities scans at 1° elevation angle from DOW7 at a) 2156:08. b) 2200:08, c) 2202:09, d) 2204:08, e) 2206:10, f) 2208:11, g) 2210:10, h) 2212:10, i) 2214:09, and j) 2216:07 UTC. Gray lines denote the range and elevation angle grid. The red range ring denotes the location of vertical cross sections shown in Figs. 3-8. The letter "X" plotted on the reflectivity scan in a) is shown in Fig. 3.

ground and aerial survey identified tornadic damage at ~2152 (Fig. 1) well before the appearance of a funnel cloud. The operators of the DOW7 radar, independently, reported tornadogenesis at 2152 based on the strength of the rotation couplet compared with numerous past intercepts of tornadic storms.

The locations of four photographs taken of the tornado (Fig. 1) are shown by letter identifies along the track. As previously mentioned, azimuth- and elevation-angle grids were superimposed onto all pictures presented in this paper. A difficulty often encountered when comparing storm-intercept photographs are the different camera locations, focal length of the lens, and

varying distances to the tornado. These factors can lead to erroneous perceived changes in the funnel width, for example. The superimposed photogrammetric angles on the pictures and the exact radial distance to the tornado based on the radar data provided a solution to this problem. This information was used to either enlarge or reduce the pictures so that the relative dimensions of the tornado were equal as shown in Fig. 1 and other figures presented in this paper. These adjustments allow for a direct comparison of the tornado dimensions between photos. The largest funnel width at 2209:58 was ~600 m just below cloud base in Fig. 1.

3. VERTICAL CROSS SECTIONS THROUGH THE TORNADO

The high-resolution radar data was combined with a series of still photographs in an attempt to document the evolution of the tornado's visual structure in relation to the radar reflectivity and Doppler velocity fields. The range to the rotational couplet was determined using single-Doppler velocity data from DOW7. At these ranges, which in some cases varied by a few range rates at different elevation angles, pseudo-vertical cross sections were assembled through the center of the WEH and the rotational couplet. These cross sections are along curved surfaces (i.e., constant range) as shown in Fig. 2. The first analysis time was at ~2156 and the last analysis time was ~2217.

a. 2156:08-2156:45

Two series of cross sections were created for each radar volume scan. One was based on a wide-angle view of the visual features below cloud base and second was a magnified view that would reveal the details of the developing and mature stages of the tornadic circulation. The wall cloud and a funnel aloft are apparent during the first volume scan at 2156:08-2156:45 (Fig. 3). The southern edge (left in the picture) of the wall cloud was ~400 m below cloud base and the lower tip of the funnel was ~200 m above ground level (AGL; hereafter, all heights are AGL). A rain shaft was located north of the funnel cloud (281°-283° azimuth) and was embedded in radar reflectivity >50 dBZ. The location of the curtain of precipitation that connects the hook echo with the main storm is shown (label "X") in Figs. 2a and 3b. This curtain is positioned near the southern edge of the wall cloud (Fig. 3b) where precipitation was not visually apparent even though the values of radar reflectivity were between 40-50 dBZ. This observation suggests that the echo return could have been a result of a sparse collection of large hydrometeors.

An enlargement of the analysis at 2156:08-2156:45 centered on the funnel cloud is shown in Fig. 4. The positions of the raw values of radar reflectivity and Doppler velocity are plotted as dots on Figs. 4a and b. Estimating the resolvable scales is important in the present case since the hook echo was approaching the DOW7 radar (Fig. 1). Accordingly, the DOW7 radar beamwidth has been added to all vertical cross sections shown in this section.

b. 2206:10-2206:46

The azimuthal shear began to increase dramatically after ~2205 and was accompanied by the development of a funnel cloud that reached the surface (Fig. 5). The visual appearance of the precipitation encompassing the funnel (Fig. 5) is consistent with the tube of high reflectivity surrounding the WEH (Figs. 2e and 5b). Note that the 50 dBZ isopleths are >1 km from the funnel and are located near the north and south edges of the precipitation shaft. The diameter of WEH (~600 m) was much larger than the funnel. The region of radar reflectivity <15 dBZ extends to a higher altitude suggesting that centrifuging of hydrometeors increased owing to stronger rotation. A major structural change within the WEH near the surface has occurred during this time. The radar reflectivities are now greater 20 dBZ and the minimum radar reflectivities denoted by the 15 dBZ contour are now aloft (the minimum reflectivities were located at the surface at earlier analysis times). This increase in echo intensity at low levels may have been a result of lofted debris from the surface although none was visual apparent in the photograph. The strongest circulation associated with the tornado is concentrated in the lowest few hundred meters as indicated by the intense positive and negative values of Doppler velocity (Figs. 5c and 6b).

c. 2212:10-2212:46

The tornado is embedded in heavy precipitation as shown in the wide-angle photograph taken at 2211:58 (Fig. 7). There is good agreement between the precipitation seen in the photograph and the superimposed echo associated with hook echo (Figs. 2h and 7b). Note the agreement of the slope of the isopleths of radar reflectivity between 267°-271° and the precipitation shaft in the same region. The increase of the radar reflectivity within the WEH at low levels has continued with echoes >45 dBZ centered at the location of the funnel (Figs. 7b and 8a). The resultant structure can be described as a couplet of high/low radar reflectivity in the vertical. This increase in echo return within the WEH with time can also be seen by comparing the low-level scans shown in Figs. 2f-j. This is, once again, suggestive of debris being lofted from the ground (debris does seem to be apparent from 281°-282° in Fig. 8a).

The rotational couplet at low levels continues to intensify with velocities now <-50 ms^{-1} and >30 m s^{-1} toward and away from the radar, respectively (Figs. 7c and 8b). The rotational speeds first decrease above this level before increasing in strength between 5°-6° in elevation angle (Fig. 8b).

d. Double ring structure within the hook echo

Wurman and Gill (2000) were among the first to report a double ring structure within a hook echo. They proposed that the inner ring was associated with debris lofted from the ground while the outer ring was associated with precipitation. Additional reports in the

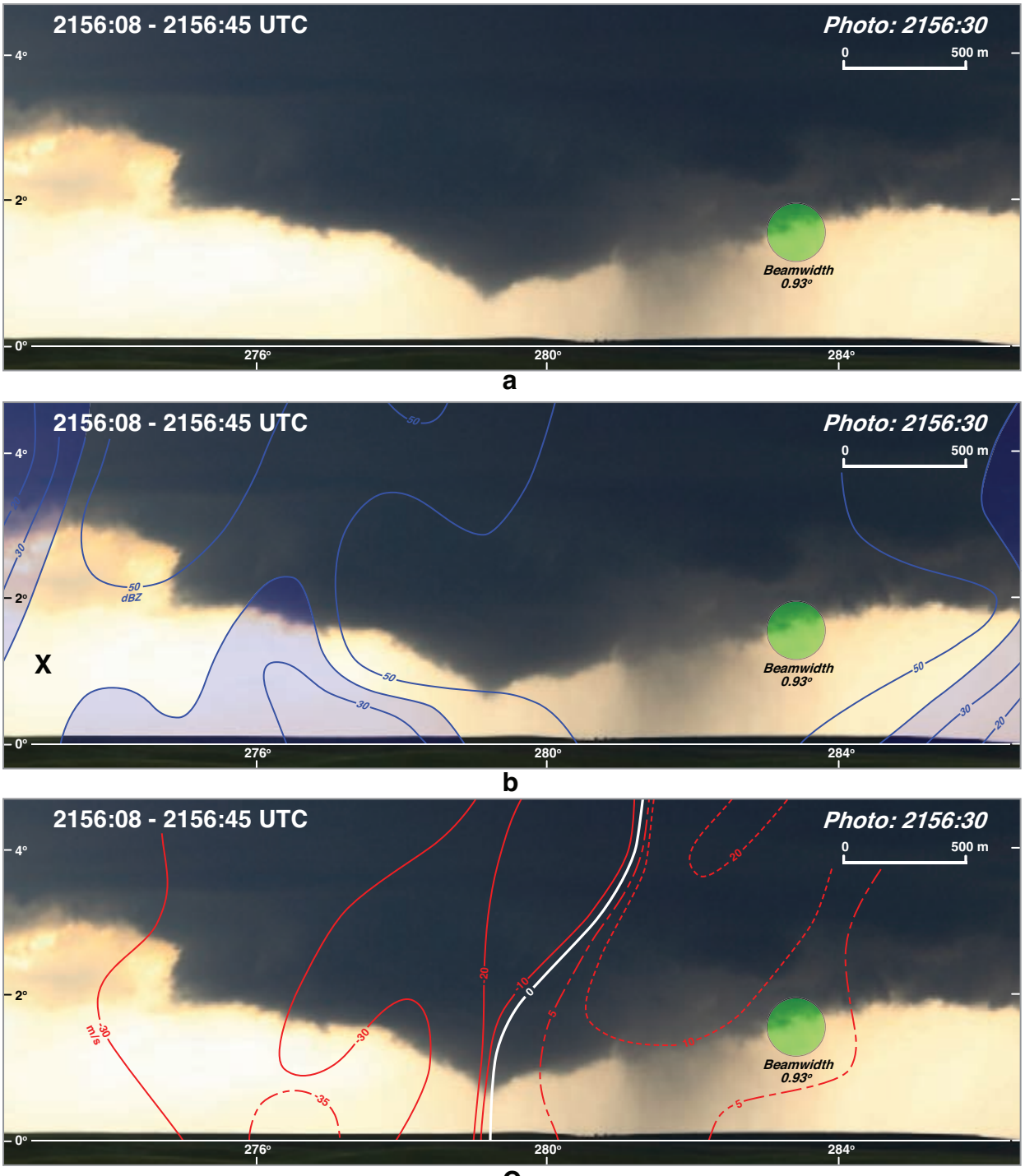

Fig. 3. Wide angle photograph of the La Grange tornado at 2156:30 UTC. Blue lines in b) are isopleths of radar reflectivity with values less than 40 dBZ shaded light blue. Red lines in c) are isopleths of single-Doppler velocity. Solid and dashed lines represent negative and positive velocities, respectively. Additional isopleths of Doppler velocities have been added (dashed-dot lines) in weak gradient regions. The green circle represents the beamwidth of the radar. The scale labeled in the figures are valid at the distance of the tornado. All wide-angle photographs have been enlarged or reduced so that the scales are equivalent (i.e., the relative dimensions of the tornado are equal when comparing photographs shown in these figures). The letter "X" labeled on b) is shown in Fig. 2.

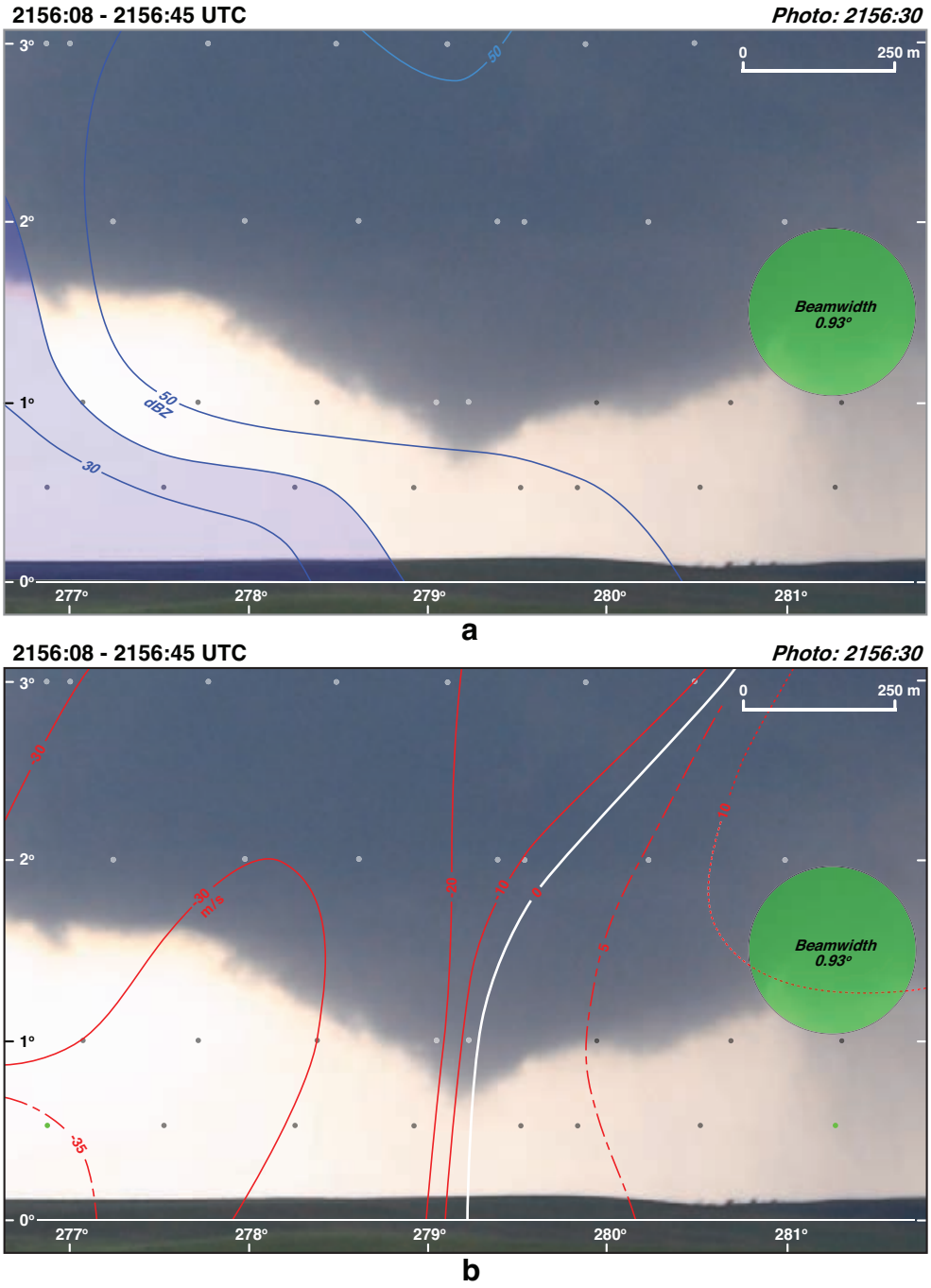

Fig. 4. Enlarged photograph of the La Grange tornado at 2156:30 UTC. Blue lines in a) are isoplths of radar reflectivity with values less than 40 dBZ shaded light blue. Red lines in b) are isopleths of single-Doppler velocity. Solid and dashed lines represent negative and positive velocities, respectively. Additional isopleths of Doppler velocities have been added (dashed-dot lines) in weak gradient regions. The green circle represents the beamwidth of the radar. The scale labeled in the figures are valid at the distance of the tornado. All zoomed-in photographs have been enlarged or reduced so that the scales are equivalent (i.e., the relative dimensions of the tornado are equal when comparing photographs shown in these figures). The small dots represents the raw data points from DOW7.

literature of a double ring structure include Wurman et al. (2007a) and Tanamachi et al. (2007). Bluestein et al. (2007b) used dual-polarization measurements at X-band to show that the inner ring of a hook echo was likely the result of debris particles.

DOW7 recorded a double ring structure in the low-level scans of the LaGrange tornado from 2216:51-2217:06 (Fig. 9a). The scan at 2° clearly shows an inner ring with a small WEH embedded within the larger hook echo and the funnel cloud. The small WEH is not

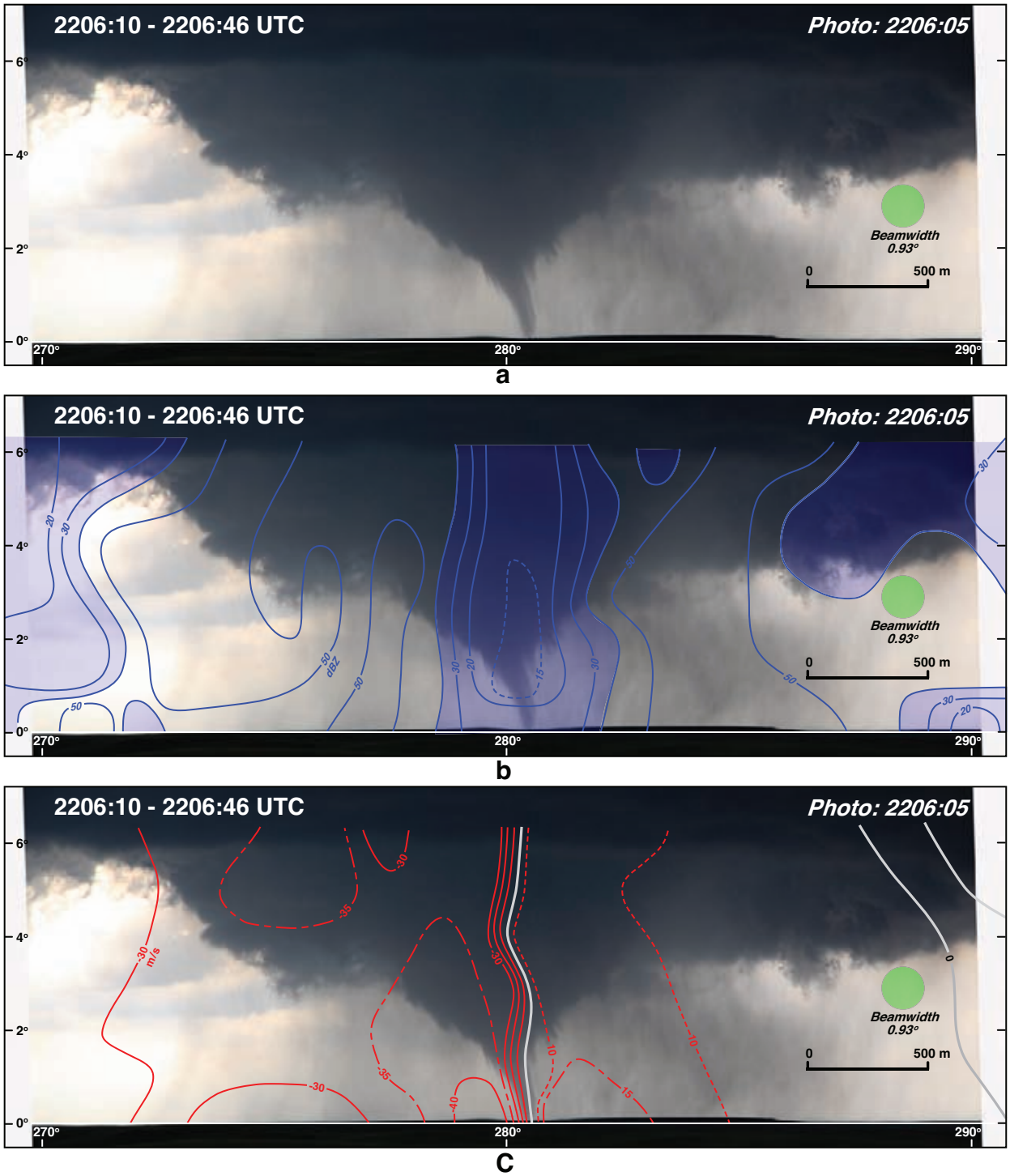

Fig. 5. Wide angle photograph of the La Grange tornado at 2206:05 UTC. Contour description is the same as Fig. 3.

apparent at 0.5°. The velocity differential across the tornado was ~105 m s^{-1} at this time (Fig. 9d). The weak echo trench surrounding the inner ring is denoted by the letter identifiers in Figs. 9a and c. There is a reduction in the diameter of this trench with increasing height (the radar did not scan the tornado at the 3° and 4° elevation angles). It appears that debris, visually apparent between 272°-278° (Fig. 9b), is associated with radar reflectivities >45 dBZ. Dowell et al. (2005) proposed that lofted debris and hydrometeors exhibit outward motion within a matter of a few tens of seconds. This results in a decrease in their number concentration within the tornado core (i.e., the appearance of a WEH) and increases their concentration somewhat outside the core. This scenario

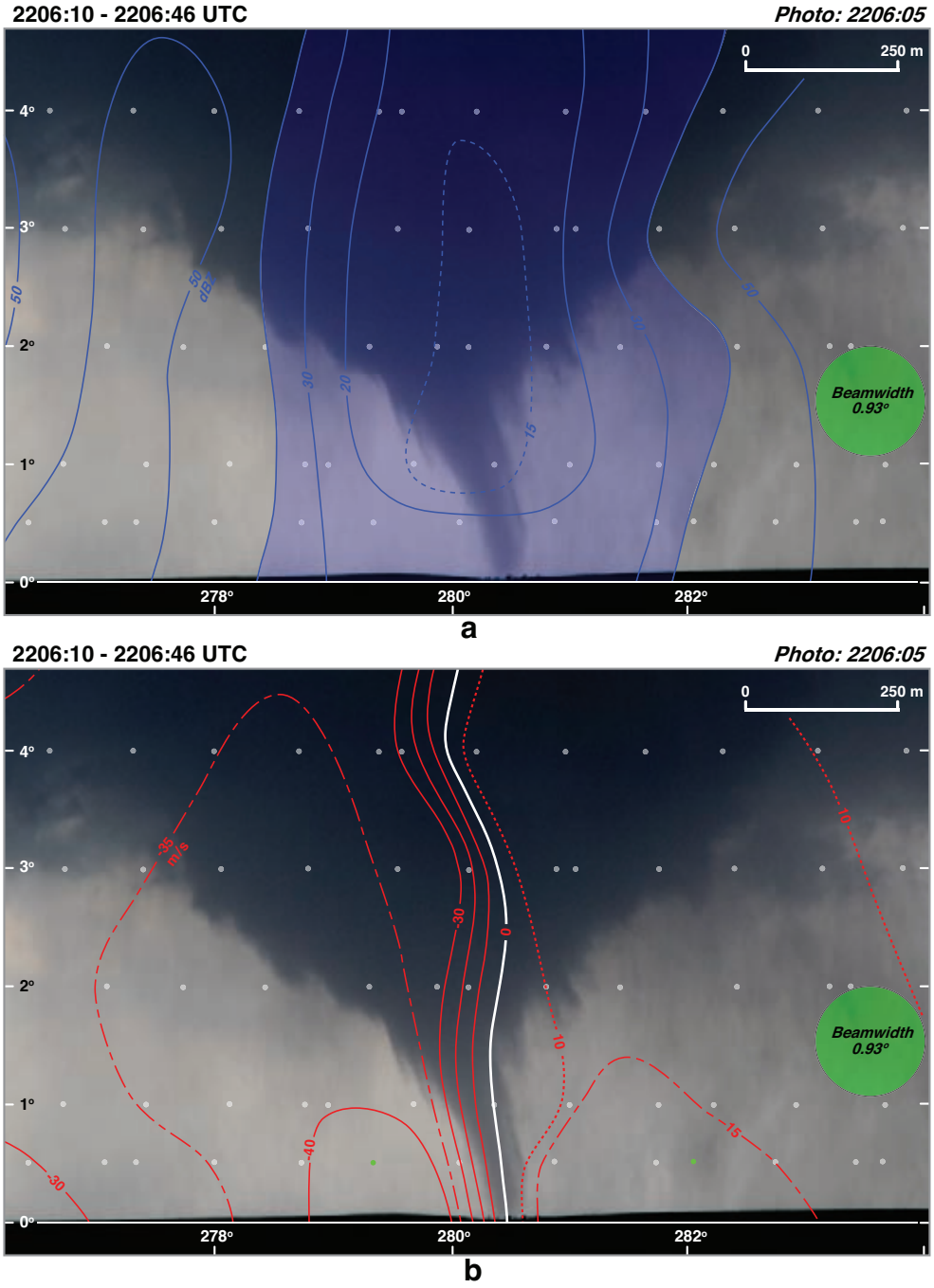

Fig. 6. Enlarged photograph of the La Grange tornado at 2206:05 UTC. Contour description is the same as Fig. 4.

would describe the echo pattern shown in Fig. 9c.

.

6. SUMMARY AND DISCUSSION

The current study presents a single-Doppler radar analysis combined with cloud photography of the LaGrange tornado on 5 June 2009 in an attempt to relate the hook echo, weak-echo hole (WEH), and rotational couplet to the visual characteristics of the tornado. The DOW radars set up out ahead of the supercell storm along a north-south highway. The radars collected high resolution data on the wall cloud and the tornado. The tornado damage was not extensive based on a post-storm survey and led to EF2 rating. Tornadogenesis is believed to have occurred at 2152 based on the confirmed tornadic damage at the ground combined with the single-Doppler velocities within the rotational couplet observed by the DOW radar.

A WEH within the hook echo began to form

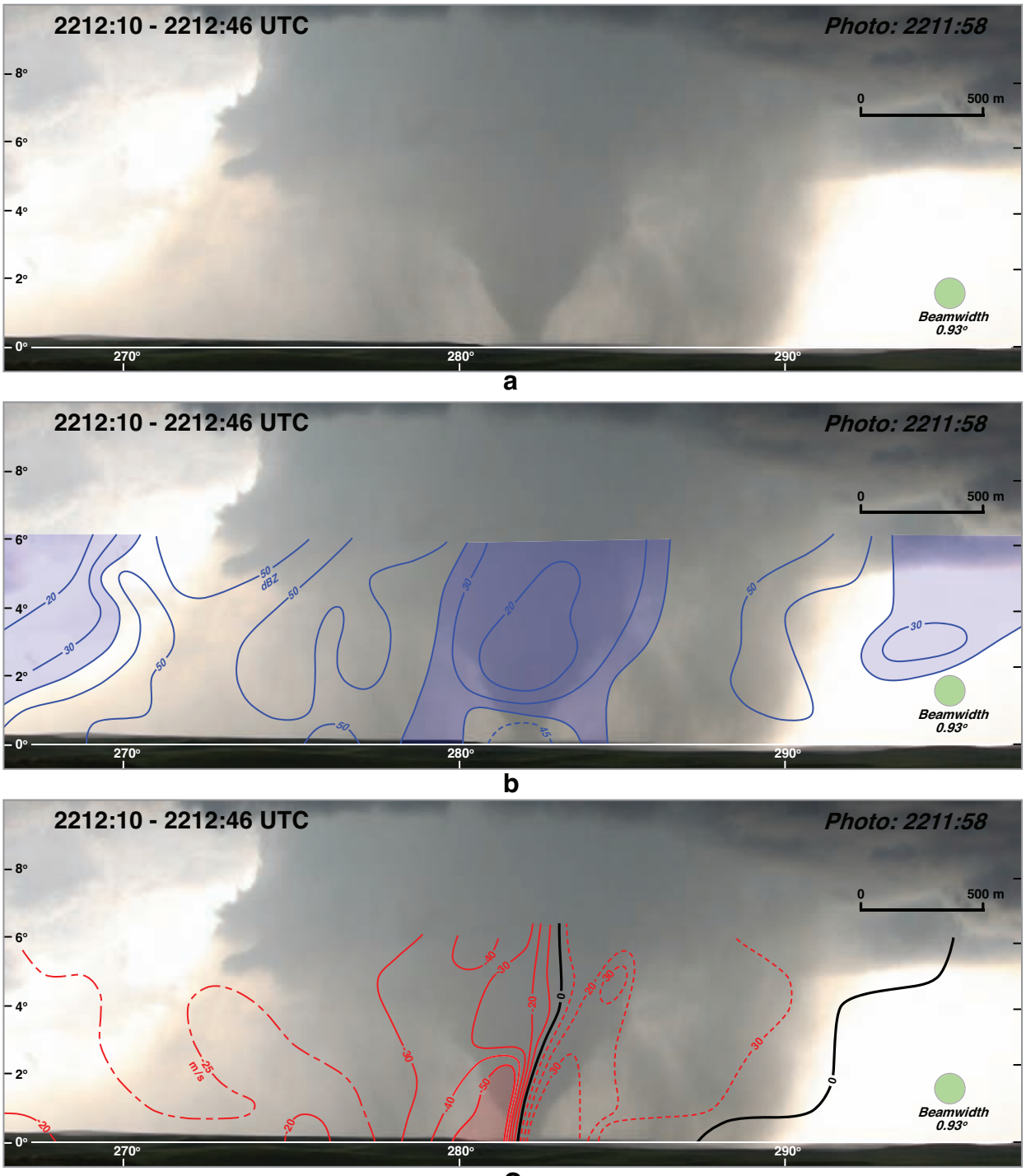

Fig. 7. Wide angle photograph of the La Grange tornado at 2211:58 UTC. Contour description is the same as Fig. 3.

at 2158 and was clearly apparent by 2200 before the appearance of a funnel cloud. Dowell et al. (2005) proposed that a distinctive tornadic signature is the presence of a WEH within the hook and a tube of high reflectivity that is tapered near the surface. The tornado is often associated with higher reflectivity near the surface. In contrast, Bluestein et al. (2004) described a pear-shaped echo structure near the surface. In addition, bulges in the WEH have been reported by Bluestein et al. (2007a).

The echo pattern through the hook echo on 5 June undergoes a dramatic evolution. Initially, the minimum radar reflectivities are near the surface (<15 dBZ) and the WEH does not suggest a tapered structure near the ground. Subsequently, higher reflectivities appear near the surface when the funnel cloud makes

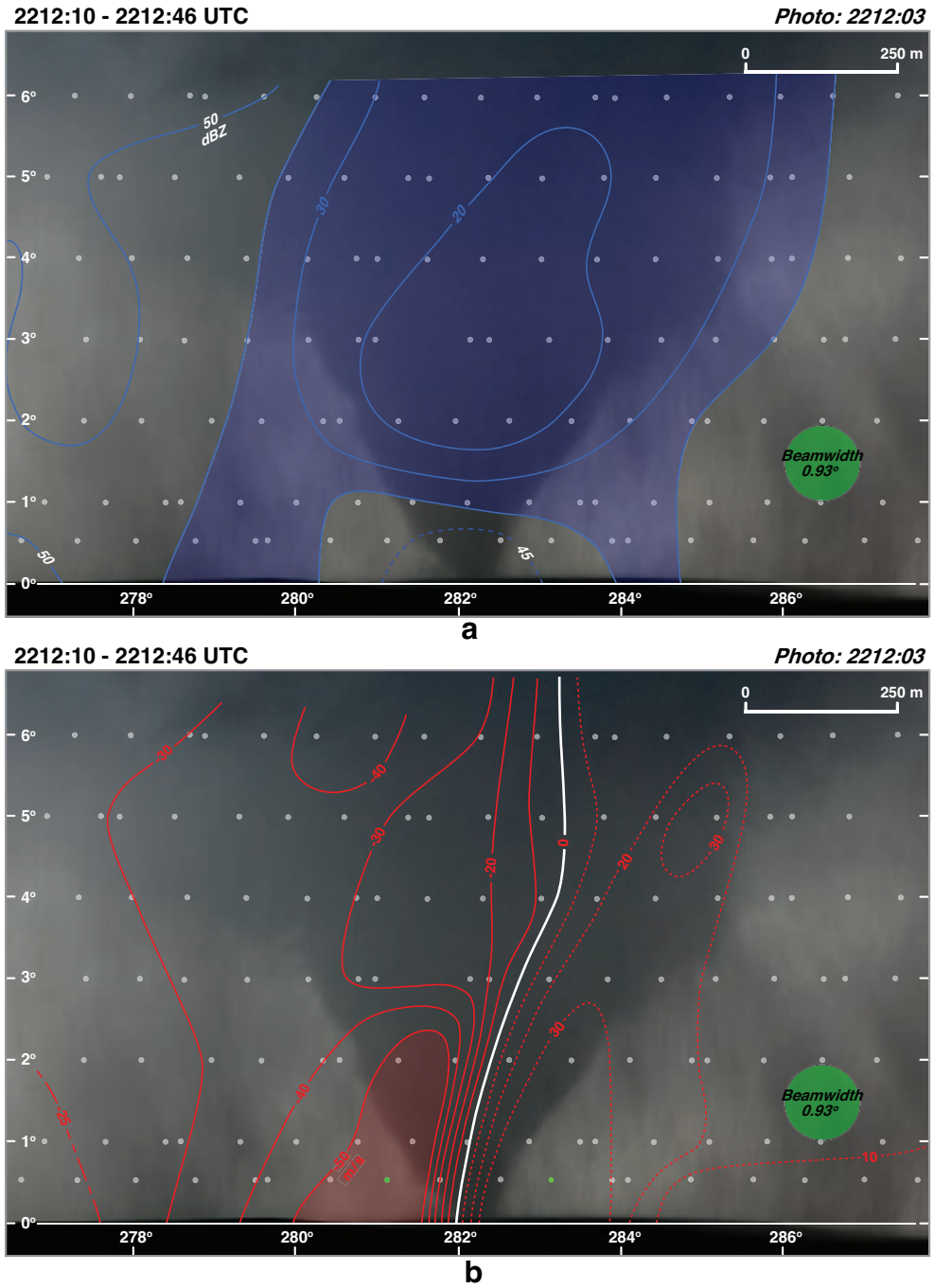

Fig. 8. Enlarged photograph of the La Grange tornado at 2212:03 UTC. Contour description is the same as Fig. 4.

"contact" with the ground. During one analysis time, the increase of the radar reflectivity within the WEH at low levels results in a couplet of high/low radar reflectivity in the vertical. This increase in echo at low levels is believed to be associated with lofted debris although none was visibly apparent until the last analysis time. The WEH was nominally wider that the visible funnel cloud.

The data set provided the first detailed analysis of the double ring structure within a hook echo that has been reported in a several studies. The inner high reflectivity region is believed to be a result of lofted debris. At higher elevation angles, a small WEH appeared within the high reflectivity region owing to centrifuging of debris as schematically shown in Fig. 10.

Acknowledgements. The National Center for Atmospheric Research is sponsored by the National Science Foundation. Any opinions, findings and conclusions or recommendations expressed in this publication are those of the authors and do not necessarily reflect the views of the National Science Foundation. Research re-

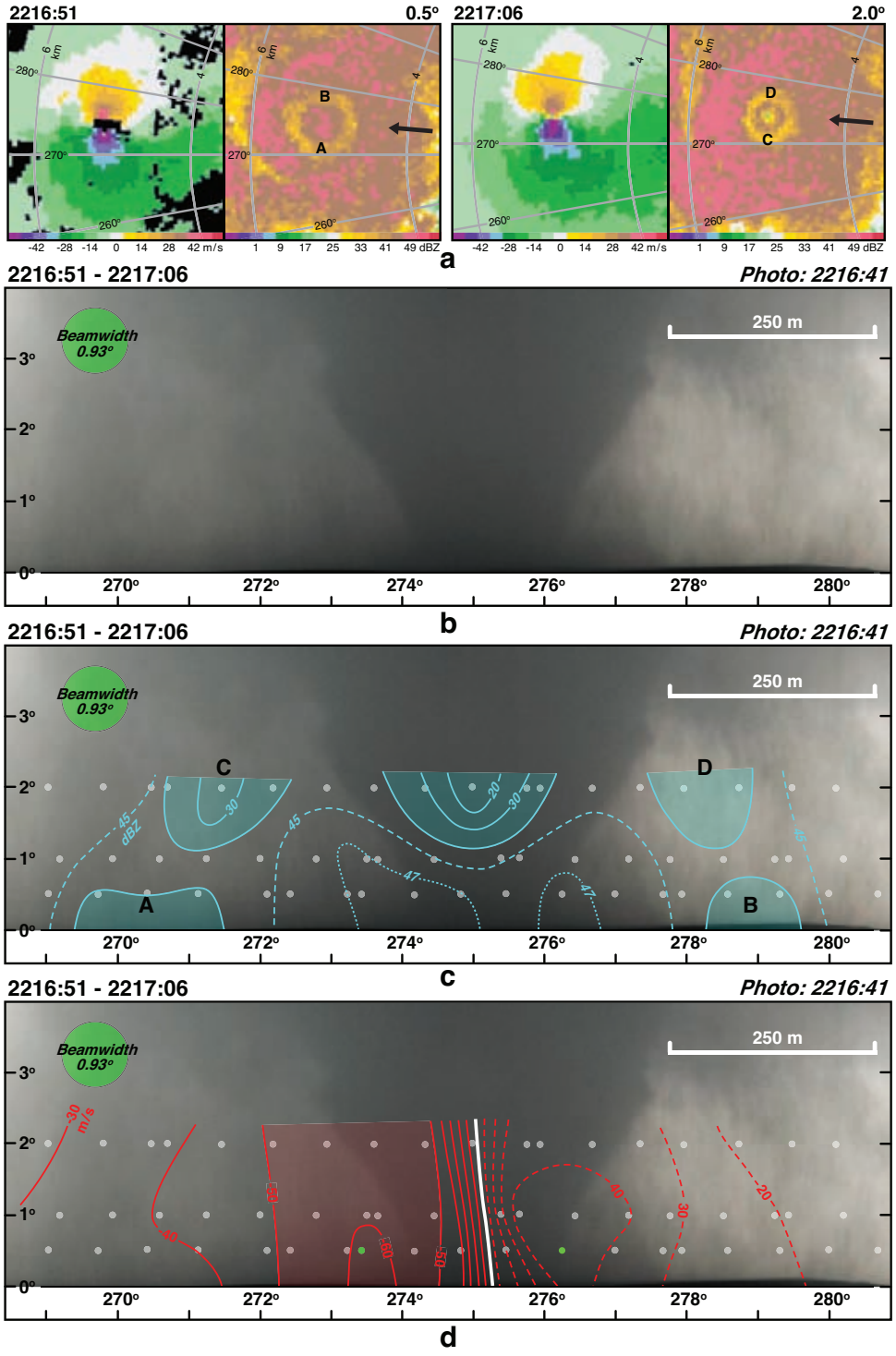

Fig. 9. a) Low-level scans of Doppler velocity and radar reflectivity at 0.5° and 2° recorded by DOW7. b) Photograph of the La Grange Tornado at 2216:41 UTC. c) Radar reflectivity superimposed onto the photograph. Values less than 40 dBZ shaded light blue. d) Single-Doppler velocities superimposed onto the photograph. Solid and dashed lines represent negative and positive velocities, respectively. Values less than -50 m s^{-1} shaded light red. The green circle represents the beamwidth of the radar. Letter identifiers denoting the position of the weak echo region are shown in a and c. The scale labeled in the figures are valid at the distance of the tornado. The small dots represents the raw data points from DOW7.

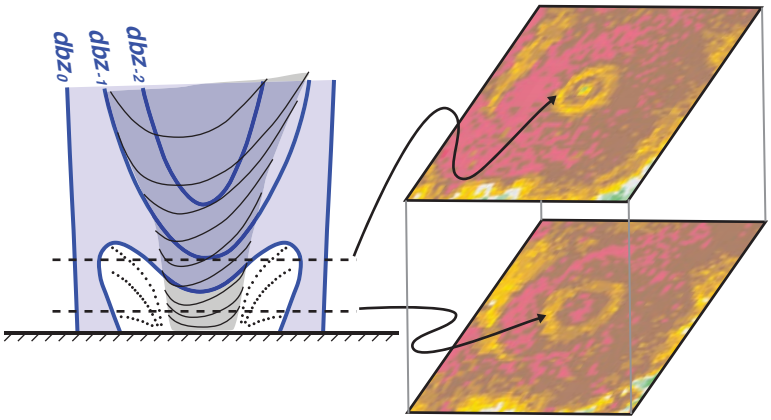

Fig. 10. Schematic models summarizing some of the observations from the La Grange tornado. Vertical profile of radar reflectivity through the inner ring of the hook echo. The black dashed lines represent the locations of scans through the tornado. Hypothetical low level scans of radar reflectivity are shown by the the 2 images on the right. Low values of radar reflectivity are shaded light blue.

sults presented in this paper were supported by the National Science Foundation under Grants ATM-0757714. The DOW radars are National Science Foundation Lower Atmospheric Observing Facilities supported by ATM-0734001. The DOW deployments in VORTEX2 have been supported by ATM-0910737 and ATM-0966095. Analysis of DOW data has been supported by ATM-0947235. VORTEX2 has been supported, in part, by ATM-0724318.

REFERENCES

Alexander, C.R., and J. Wurman, 2005: The 30 May 1998 Spencer, South Dakota storm. Part I: The structural evolution and environment of the tornadoes. *Mon. Wea. Rev.*, **133,** 72-96.

Bluestein, H.B., J.G. LaDue, H. Stein, D. Speheger, and W.P. Unruh, 1993: Doppler radar wind spectra of supercell tornadoes. *Mon. Wea. Rev.*, **121,** 2200-2221.

_____, W.P. Unruh, D.C. Dowell, T.A. Hutchinson, T.M. Crawford, A.C. Wood, H. Stein, 1997: Doppler radar analysis of the Northfield, Texas, tornado of 25 May 1994. *Mon. Wea. Rev.*, **125,** 212-230.

_____, C.C. Weiss, A.L. Pazmany, 2004: The vertical structure of a tornado near Happy, Texas, on 5 May 2002: High-resolution, mobile, W-band, Doppler radar observations. *Mon. Wea. Rev.*, **132,** 2325-2337.

_____, C.C. Weiss, M.M. French, E.M. Holthaus, R.L. Tanamachi, S. Frasier, and A.L. Pazmany, 2007a: The structure of tornadoes near Attica, Kansas, on 12 May 2004: High-resolution, mobile, Doppler radar observations. *Mon. Wea. Rev.*, **135,** 475-506.

_____, M.M. French, R.L. Tanamachi, S. Frazier, K. Hardwick, F. Junyent, and A.L. Pazmany, 2007b: Close-range observations of tornadoes in supercells made with a dual-polarization, X-band, mobile Doppler radar. *Mon. Wea. Rev.*, **135,** 1522-1543.

_____, D. Burgess, D. Dowell, P. Markowski, E. Rasmussen, Y. Richardson, L. Wicker, and J. Wurman, 2009: VORTEX2: The second verification of the origins of rotation in tornadoes experiment. Preprints, *5th European Conference on Severe Local Storms*, Landshut, Germany, O09-06.

Brown, R.A., L.R. Lemon, and D.W. Burgess, 1978: Tornado detection by pulsed Doppler radar. *Mon. Wea., Rev.*, **106,** 29-38.

Dowell, D.C., C.R. Alexander, J.M. Wurman, and L.J. Wicker, 2005: Centrifuging of hydrometeors and debris in tornadoes: Radar-reflectivity patterns and wind-measurement errors. *Mon. Wea. Rev.*, **133,** 1501-1524.

Forbes, G.S., 1981: On the reliability of hook echoes as tornado indicators. *Mon. Wea. Rev.*, **109,** 1457-1466.

Fujita, T.T., 1981: Tornadoes and downbursts in the context of generalized planetary scales. *J. Atmos. Sci.*, **38,** 1511-1534.

Rasmussen, E., and J.M. Straka, 2007: Evolution of low-level angular momentum in the 2 June 1995 Dimmitt, Texas, tornado cyclone. *J. Atmos. Sci.*, **62,** 2037-2057.

Stout, G.E., and F.A. Huff, 1953: Radar records Illinois tornadogenesis. *Bull. Amer. Meteor. Soc.*, **34,** 281-284.

Tanamachi, R.L., H.B. Bluestein, W.-C. Lee, M. Bell, and A. Pazmany, 2007: Ground-based velocity track display (GBVTD) analysis of W-band Doppler radar data in a tornado near Stockton, Kansas, on 15 May 1999. *Mon. Wea. Rev.*, **135,** 783-800.

Wakimoto, R.M., and B.E. Martner, 1992: Observations

of a Colorado tornado. Part II: Combined photogrammetric and Doppler radar analysis. *Mon. Wea. Rev.*, **120,** 522-543.

_____, W.-C., Lee, H.B. Bluestein, C.-H. Liu, and P.H. Hildebrand, 1996: ELDORA observations during VORTEX 95. *Bull. Amer. Meteor. Soc.*, **77,** 1465-1481.

_____, H.V. Murphey, D.C. Dowell, and H.B. Bluestein, 2003: The Kellerville tornado during VORTEX: Damage survey and Doppler radar analyses. *Mon. Wea. Rev.*, **131,** 2197-2221.

Wurman, J., and S. Gill, 2000: Finescale radar observations of the Dimmitt, Texas (2 June 1995), tornado. *Mon. Wea. Rev.*, **128,** 2135-2164.

_____, J.M. Straka, and E.N. Rasmussen, 1996: Fine-scale Doppler radar observations of tornadoes. *Science*, **272,** 1774-1777.

_____, Y. Richardson, C. Alexander, S. Weygandt, and P.F. Zhang, 2007a: Dual-Doppler and single-Doppler analysis of a tornadic storm undergoing mergers and repeated tornadogenesis. *Mon. Wea. Rev.*, **135,** 736-758.

_____, _____, _____, _____, and _____, 2007b: Dual-Doppler analysis of winds and vorticity budget terms near a tornado. *Mon. Wea. Rev.*, **135,** 2392-2405.